Monthly Notices
of the
ROYAL ASTRONOMICAL SOCIETY

MNRAS **439,** 2828–2836 (2014)
Advance Access publication 2014 February 11

doi:10.1093/mnras/stu139

HESS J1640−465 – an exceptionally luminous TeV γ-ray supernova remnant

HESS Collaboration, A. Abramowski,[1] F. Aharonian,[2,3,4] F. Ait Benkhali,[2] A. G. Akhperjanian,[4,5] E. Angüner,[6] G. Anton,[7] S. Balenderan,[8] A. Balzer,[9,10] A. Barnacka,[11] Y. Becherini,[12] J. Becker Tjus,[13] K. Bernlöhr,[2,6] E. Birsin,[6] E. Bissaldi,[14] J. Biteau,[15] M. Böttcher,[16] C. Boisson,[17] J. Bolmont,[18] P. Bordas,[19] J. Brucker,[7] F. Brun,[2] P. Brun,[20] T. Bulik,[21] S. Carrigan,[2] S. Casanova,[2,16] M. Cerruti,[17]★ P. M. Chadwick,[8] R. Chalme-Calvet,[18] R. C. G. Chaves,[20] A. Cheesebrough,[8] M. Chrétien,[18] S. Colafrancesco,[22] G. Cologna,[23] J. Conrad,[24]† C. Couturier,[18] Y. Cui,[19] M. Dalton,[25]‡ M. K. Daniel,[8] I. D. Davids,[16,26] B. Degrange,[15] C. Deil,[2] P. deWilt,[27] H. J. Dickinson,[24] A. Djannati-Ataï,[28] W. Domainko,[2] L. O'C. Drury,[3] G. Dubus,[29] K. Dutson,[30] J. Dyks,[11] M. Dyrda,[31] T. Edwards,[2] K. Egberts,[14] P. Eger,[2] P. Espigat,[28] C. Farnier,[24] S. Fegan,[15] F. Feinstein,[32] M. V. Fernandes,[1] D. Fernandez,[32] A. Fiasson,[33] G. Fontaine,[15] A. Förster,[2] M. Füßling,[10] M. Gajdus,[6] Y. A. Gallant,[32] T. Garrigoux,[18] G. Giavitto,[9] B. Giebels,[15] J. F. Glicenstein,[20] M.-H. Grondin,[2,23] M. Grudzińska,[21] S. Häffner,[7] J. Hahn,[2] J. Harris,[8] G. Heinzelmann,[1] G. Henri,[29] G. Hermann,[2] O. Hervet,[17] A. Hillert,[2] J. A. Hinton,[30] W. Hofmann,[2] P. Hofverberg,[2] M. Holler,[10] D. Horns,[1] A. Jacholkowska,[18] C. Jahn,[7] M. Jamrozy,[34] M. Janiak,[11] F. Jankowsky,[23] I. Jung,[7] M. A. Kastendieck,[1] K. Katarzyński,[35] U. Katz,[7] S. Kaufmann,[23] B. Khélifi,[28] M. Kieffer,[18] S. Klepser,[9] D. Klochkov,[19] W. Kluźniak,[11] T. Kneiske,[1] D. Kolitzus,[14] Nu. Komin,[33] K. Kosack,[20] S. Krakau,[13] F. Krayzel,[33] P. P. Krüger,[16,2] H. Laffon,[25] G. Lamanna,[33] J. Lefaucheur,[28] A. Lemière,[28] M. Lemoine-Goumard,[25] J.-P. Lenain,[18] D. Lennarz,[2] T. Lohse,[6] A. Lopatin,[7] C.-C. Lu,[2] V. Marandon,[2] A. Marcowith,[32] R. Marx,[2] G. Maurin,[33] N. Maxted,[27] M. Mayer,[10] T. J. L. McComb,[8] J. Méhault,[25]§ P. J. Meintjes,[36] U. Menzler,[13] M. Meyer,[24] R. Moderski,[11] M. Mohamed,[23] E. Moulin,[20] T. Murach,[6] C. L. Naumann,[18] M. de Naurois,[15] J. Niemiec,[31] S. J. Nolan,[8] L. Oakes,[6] S. Ohm,[30]§ E. de Oña Wilhelmi,[2] B. Opitz,[1] M. Ostrowski,[34] I. Oya,[6] M. Panter,[2] R. D. Parsons,[2] M. Paz Arribas,[6] N. W. Pekeur,[16] G. Pelletier,[29] J. Perez,[14] P.-O. Petrucci,[29] B. Peyaud,[20] S. Pita,[28] H. Poon,[2] G. Pühlhofer,[19] M. Punch,[28] A. Quirrenbach,[23] S. Raab,[7] M. Raue,[1] A. Reimer,[14] O. Reimer,[14] M. Renaud,[32] R. de los Reyes,[2] F. Rieger,[2] L. Rob,[37] C. Romoli,[3] S. Rosier-Lees,[33] G. Rowell,[27] B. Rudak,[11] C. B. Rulten,[17] V. Sahakian,[5,4] D. A. Sanchez,[2,33] A. Santangelo,[19] R. Schlickeiser,[13]

★ Now at Harvard–Smithsonian Center for Astrophysics, 60 Garden Street, Cambridge, MA 02138, USA.
† Wallenberg Academy Fellow.
‡ Funded by contract ERC-StG-259391 from the European Community.
§ E-mail: so100@le.ac.uk

F. Schüssler,[20] A. Schulz,[9] U. Schwanke,[6] S. Schwarzburg,[19] S. Schwemmer,[23] H. Sol,[17] G. Spengler,[6] F. Spies,[1] Ł. Stawarz,[34] R. Steenkamp,[26] C. Stegmann,[10,9] F. Stinzing,[7] K. Stycz,[9] I. Sushch,[6,16] A. Szostek,[34] J.-P. Tavernet,[18] T. Tavernier,[28] A. M. Taylor,[3] R. Terrier,[28] M. Tluczykont,[1] C. Trichard,[33] K. Valerius,[7] C. van Eldik,[7] B. van Soelen,[36] G. Vasileiadis,[32] C. Venter,[16] A. Viana,[2] P. Vincent,[18] J. Vink,[38] H. J. Völk,[2] F. Volpe,[2] M. Vorster,[16] T. Vuillaume,[29] S. J. Wagner,[23] P. Wagner,[6] M. Ward,[8] M. Weidinger,[13] Q. Weitzel,[2] R. White,[30] A. Wierzcholska,[34] P. Willmann,[7] A. Wörnlein,[7] D. Wouters,[20] V. Zabalza,[2] M. Zacharias,[13] A. Zajczyk,[11,32] A. A. Zdziarski,[11] A. Zech[17] and H.-S. Zechlin[1]

[1] *Universität Hamburg, Institut für Experimentalphysik, Luruper Chaussee 149, D-22761 Hamburg, Germany*
[2] *Max-Planck-Institut für Kernphysik, PO Box 103980, D-69029 Heidelberg, Germany*
[3] *Dublin Institute for Advanced Studies, 31 Fitzwilliam Place, Dublin 2, Ireland*
[4] *National Academy of Sciences of the Republic of Armenia, 24, Marshall Baghramian Avenue, 0019 Yerevan, Armenia*
[5] *Yerevan Physics Institute, 2 Alikhanian Brothers St, 375036 Yerevan, Armenia*
[6] *Institut für Physik, Humboldt-Universität zu Berlin, Newtonstr. 15, D-12489 Berlin, Germany*
[7] *Physikalisches Institut, Universität Erlangen-Nürnberg, Erwin-Rommel-Str. 1, D-91058 Erlangen, Germany*
[8] *Department of Physics, University of Durham, South Road, Durham DH1 3LE, UK*
[9] *DESY, D-15738 Zeuthen, Germany*
[10] *Institut für Physik und Astronomie, Universität Potsdam, Karl-Liebknecht-Strasse 24/25, D-14476 Potsdam, Germany*
[11] *Nicolaus Copernicus Astronomical Center, ul. Bartycka 18, PL-00-716 Warsaw, Poland*
[12] *Department of Physics and Electrical Engineering, Linnaeus University, SE-351 95 Växjö, Sweden*
[13] *Institut für Theoretische Physik, Lehrstuhl IV: Weltraum und Astrophysik, Ruhr-Universität Bochum, D-44780 Bochum, Germany*
[14] *Institut für Astro- und Teilchenphysik, Leopold-Franzens-Universität Innsbruck, A-6020 Innsbruck, Austria*
[15] *Laboratoire Leprince-Ringuet, Ecole Polytechnique, CNRS/IN2P3, F-91128 Palaiseau, France*
[16] *Centre for Space Research, North-West University, Potchefstroom 2520, South Africa*
[17] *LUTH, Observatoire de Paris, CNRS, Université Paris Diderot, 5 Place Jules Janssen, F-92190 Meudon, France*
[18] *LPNHE, Université Pierre et Marie Curie Paris 6, Université Denis Diderot Paris 7, CNRS/IN2P3, 4 Place Jussieu, F-75252, Paris Cedex 5, France*
[19] *Institut für Astronomie und Astrophysik, Universität Tübingen, Sand 1, D-72076 Tübingen, Germany*
[20] *DSM/Irfu, CEA Saclay, F-91191 Gif-Sur-Yvette Cedex, France*
[21] *Astronomical Observatory, The University of Warsaw, Al. Ujazdowskie 4, PL-00-478 Warsaw, Poland*
[22] *School of Physics, University of the Witwatersrand, 1 Jan Smuts Avenue, Braamfontein, 2050 Johannesburg, South Africa*
[23] *Landessternwarte, Universität Heidelberg, Königstuhl, D-69117 Heidelberg, Germany*
[24] *Oskar Klein Centre, Department of Physics, Stockholm University, Albanova University Center, SE-10691 Stockholm, Sweden*
[25] *Centre d'Études Nucléaires de Bordeaux Gradignan, Université Bordeaux 1, CNRS/IN2P3, F-33175 Gradignan, France*
[26] *Department of Physics, University of Namibia, Private Bag 13301, Windhoek, Namibia*
[27] *School of Chemistry & Physics, University of Adelaide, Adelaide, SA 5005, Australia*
[28] *APC, AstroParticule et Cosmologie, Université Paris Diderot, CNRS/IN2P3, CEA/Irfu, Observatoire de Paris, Sorbonne Paris Cité, 10, rue Alice Domon et Léonie Duquet, F-75205 Paris Cedex 13, France*
[29] *UJF-Grenoble 1 / CNRS-INSU, Institut de Planétologie et d'Astrophysique de Grenoble (IPAG) UMR 5274, F-38041 Grenoble, France*
[30] *Department of Physics and Astronomy, The University of Leicester, University Road, Leicester LE1 7RH, UK*
[31] *Instytut Fizyki Jądrowej PAN, ul. Radzikowskiego 152, PL-31-342 Kraków, Poland*
[32] *Laboratoire Univers et Particules de Montpellier, Université Montpellier 2, CNRS/IN2P3, CC 72, Place Eugène Bataillon, F-34095 Montpellier Cedex 5, France*
[33] *Laboratoire d'Annecy-le-Vieux de Physique des Particules, Université de Savoie, CNRS/IN2P3, F-74941 Annecy-le-Vieux, France*
[34] *Obserwatorium Astronomiczne, Uniwersytet Jagielloński, ul. Orla 171, PL-30-244 Kraków, Poland*
[35] *Toruń Centre for Astronomy, Nicolaus Copernicus University, ul. Gagarina 11, PL-87-100 Toruń, Poland*
[36] *Department of Physics, University of the Free State, PO Box 339, Bloemfontein 9300, South Africa*
[37] *Institute of Particle and Nuclear Physics, Faculty of Mathematics and Physics, Charles University, V Holešovičkách 2, 180 00 Prague 8, Czech Republic*
[38] *Astronomical Institute Anton Pannekoek, University of Amsterdam, PO Box 94249, NL-1090 GE Amsterdam, the Netherlands*

Accepted 2014 January 17. Received 2014 January 17; in original form 2013 October 23

ABSTRACT

The results of follow-up observations of the TeV γ-ray source HESS J1640−465 from 2004 to 2011 with the High Energy Stereoscopic System (HESS) are reported in this work. The spectrum is well described by an exponential cut-off power law with photon index $\Gamma = 2.11 \pm 0.09_{\rm stat} \pm 0.10_{\rm sys}$, and a cut-off energy of $E_{\rm c} = 6.0^{+2.0}_{-1.2}$ TeV. The TeV emission is significantly

extended and overlaps with the northwestern part of the shell of the SNR G338.3−0.0. The new HESS results, a re-analysis of archival *XMM–Newton* data and multiwavelength observations suggest that a significant part of the γ-ray emission from HESS J1640−465 originates in the supernova remnant shell. In a hadronic scenario, as suggested by the smooth connection of the GeV and TeV spectra, the product of total proton energy and mean target density could be as high as $W_{\rm p} n_{\rm H} \sim 4 \times 10^{52} (d/10{\rm kpc})^2\,{\rm erg\,cm^{-3}}$.

Key words: radiation mechanisms: non-thermal – ISM: individual objects: G338.3−0.0 – ISM: supernova remnants.

1 INTRODUCTION

Starting in 2004 the Galactic Plane Survey (Aharonian et al. 2006c) performed by the High Energy Stereoscopic System (HESS) Collaboration, using an array of imaging atmospheric Cherenkov telescopes (IACTs), led to the discovery of nearly 70 new sources in the very high energy (VHE, $E > 100$ GeV) γ-ray regime (Carrigan et al. 2013). The challenge since then has been to associate these sources with astrophysical objects seen in other wavelengths and to identify the underlying radiation mechanisms. A large fraction of the Galactic VHE γ-ray population could be associated with regions with recent star-forming activity and to objects at late stages of stellar evolution such as supernova remnants (SNRs) and the nebulae produced by powerful young pulsars (for a review, see e.g. Hinton & Hofmann 2009). In many cases where an astrophysical counterpart to the VHE γ-ray emission could be identified, however, the nature of the underlying particle population remains unclear. Highly energetic γ-ray emission could be either produced by relativistic electrons or protons (and heavier nuclei). Relativistic hadrons undergo inelastic scattering with nuclei in the interstellar medium (ISM), producing π^0-decay γ-ray emission. Ultrarelativistic electrons, on the other hand, can upscatter low-energy photons present at the acceleration site via the Inverse Compton (IC) process. In very dense media bremsstrahlung losses of electrons can significantly contribute to the generated γ-ray emission. IACTs can play a key role in identifying the underlying particle population and studying non-thermal processes in γ-ray sources by localizing the emission region and constraining the energy spectrum at very high energies.

The VHE γ-ray source HESS J1640−465 was discovered by HESS in the Galactic Plane Survey (Aharonian et al. 2006c) and is positionally coincident with the SNR G338.3−0.0 (Whiteoak & Green 1996). Using *XMM–Newton* observations, Funk et al. (2007) detected a highly absorbed extended X-ray source (XMMU J164045.4−463131) close to the geometric centre of the SNR and within the HESS source region. The X-ray and VHE γ-ray emission components were interpreted as synchrotron and IC emission from relativistic electrons in a pulsar wind nebula (PWN). Observations with *Chandra* confirmed the presence of the extended nebula and identified a point-like source which was suggested to be the associated pulsar (Lemiere et al. 2009). Recently, Castelletti et al. (2011) analysed new high-resolution multifrequency radio data of G338.3−0.0 but could only set upper limits on the radio flux from a potential extended radio nebula. *Fermi* Large Area Telescope (LAT) observations revealed a high-energy (HE, 100 MeV $< E <$ 100 GeV) γ-ray source coincident with HESS J1640−465 (Slane et al. 2010), also designated 2FGL 1640.5−4633 in the two-year *Fermi*-LAT catalogue (Nolan et al. 2012). Note that no pulsation has been found in any wavelength band so far. Due to the large γ-ray to X-ray ratio luminosity ($L_\gamma / L_X \simeq 30$; Funk et al. 2007), Slane et al. (2010) inferred an evolved PWN with a low magnetic field and an injection spectrum that consists of a Maxwellian electron population with a power-law tail (as e.g. proposed by Spitkovsky 2008) to reproduce the broad-band spectral energy distribution (SED) in a leptonic PWN scenario. A hadronic origin of the γ-ray emission was considered to be unlikely as it would require rather high ambient densities ($n \simeq 100\ {\rm cm^{-3}}$), implying intense thermal radiation in X-rays from the SNR shell that has so far not been detected.

Lemiere et al. (2009) performed a detailed study of the gaseous environment of G338.3−0.0 and, based on the H I absorption features, derived a distance of (8–13) kpc. A recent study of the nearby stellar cluster Mercer 81 and the giant H II region G338.4+0.1 by Davies et al. (2012) supports this estimate, which implies that HESS J1640−465 is the most luminous VHE γ-ray source known in the Galaxy. Throughout this work, a distance of 10 kpc is assumed. Since the original discovery of HESS J1640−465, the available HESS exposure towards this source has quadrupled w.r.t the data used in Aharonian et al. (2006c), and advanced analysis methods are now available that allow for a much more detailed spectral and morphological study of the VHE γ-ray emission. In this work, HESS follow-up studies and a re-analysis of *XMM–Newton* data are presented. Both the broad-band SED and the TeV morphology reveal evidence for proton acceleration in the SNR shell of G338.3−0.0.

2 HESS OBSERVATIONS AND RESULTS

HESS is an array of five IACTs located in Namibia designed to detect VHE γ-rays. The fifth telescope started operation in 2012 September. All HESS data used to perform the studies described below have been taken between 2004 May and 2011 September with the four-telescope array (Aharonian et al. 2006a). The total dead-time-corrected live time amounts to 63.4 h, compared to 14.3 h in the original publication (Aharonian et al. 2006c). Observations have been performed at zenith angles between 20° and 65° with a mean value of ∼33°. The data were recorded with pointing offsets between 0.°2 and 1.°8 with a mean value of 1.°1 from the HESS J1640−465 position. Data were analysed using a standard Hillas-type HESS analysis[1] for the event reconstruction and a boosted-decision-tree-based event classification algorithm to discriminate γ-rays from the charged particle background (Ohm, van Eldik & Egberts 2009). All results were cross-checked by an independent analysis and calibration for consistency (de Naurois & Rolland 2009).

2.1 Morphology

The source position and morphology have been obtained with *hard* cuts and using the ring background estimation method (Berge,

[1] The software package HAP version 12-03-pl02 with version32 of the lookup tables was used.

Funk & Hinton 2007). In this setup, a minimum intensity in the camera image of 160 p.e. is required, resulting in an energy threshold of $E_{\rm th} = 600$ GeV and a point spread function (PSF) with 68 per cent containment radius of $r_{68} = 0.^{\circ}09$ for the morphology studies. The fit of a symmetric two-dimensional Gaussian profile, convolved with the HESS PSF with SHERPA (Freeman, Doe & Siemiginowska 2001) gives a best-fitting position of RA $16^{\rm h}40^{\rm m}41.^{\rm s}0 \pm 1.^{\rm s}0_{\rm stat} \pm 1.^{\rm s}3_{\rm sys}$ and Dec. $-46^{\circ}32'31'' \pm 14''_{\rm stat} \pm 20''_{\rm sys}$ (J2000), consistent with the previously published value (Aharonian et al. 2006c). The systematic error on the best-fitting position originates from the pointing precision of the HESS array of about 20 arcsec. The source is intrinsically extended with a Gaussian width of $\sigma_{\rm S} = (4.3 \pm 0.2)$ arcmin. This extension is 1.6 arcmin ($\sim 2\sigma$) larger than in the original publication, which can be understood as fainter emission belonging to HESS J1640−465 that can now be revealed with the increased data set. Fig. 1 shows the HESS best-fitting position and extension overlaid on the VHE γ-ray excess map. The VHE γ-ray source encloses the northern part of the SNR shell of G338.3−0.0, the candidate PWN XMMU J164045.4−463131 (Funk et al. 2007) and the *Fermi*-LAT source 2FGL 1640.5−4633 (Slane et al. 2010; Nolan et al. 2012). Fig. 1 also shows some indication for an asymmetric extension of the emission along the northern part of the shell and towards the newly discovered source HESS J1641−463 (Oya et al. 2013). This extension is also seen as residual VHE γ-ray emission when subtracting the source model from the sky map, indicating that the symmetric Gaussian model for HESS J1640−465 is an oversimplification. The residual emission could indicate some emission in between HESS J1640−465 and HESS J1641−463. This component is however not detected with high significance, making a discussion of its origin difficult in this context. Morphological fits in energy bands do not reveal any significant change in best-fitting position and/or extension, which would have indicated a change in source morphology with energy (as e.g. seen in the PWNe HESS J1825−137 or HESS J1303−631; Aharonian et al. 2006b; Abramowski et al. 2012b).

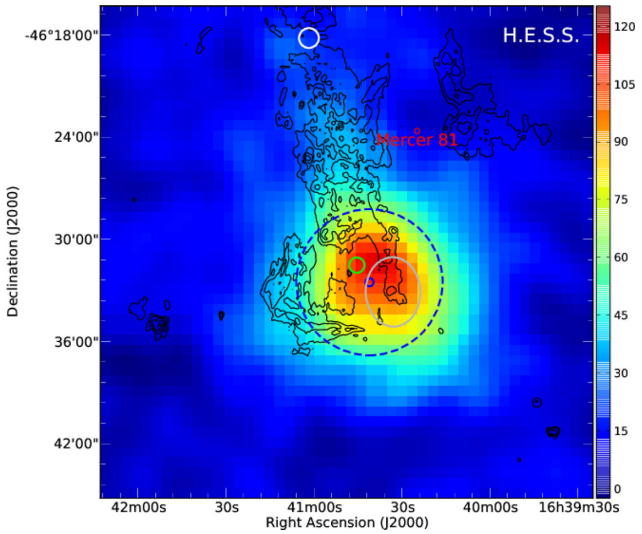

Figure 1. HESS excess map smoothed with a 2D Gaussian with $0.^{\circ}017$ variance and the best-fitting position (statistical errors only) and intrinsic Gaussian width overlaid as blue solid and dashed lines. 610 MHz radio contours are shown in black (Castelletti et al. 2011). The green circle indicates the position of the candidate PWN XMMU J164045.4−463131, and in grey, the best-fitting position of the *Fermi* source 2FGL 1640.5−4633 is given. The white circle indicates the source HESS J1641−463 (Oya et al. 2013), and the region of high radio emission connecting HESS J1640−465 and HESS J1641−463 indicates the H II region G338.4+0.1. The progenitor of G338.3−0.0 is potentially associated with the massive young stellar cluster Mercer 81 (Davies et al. 2012).

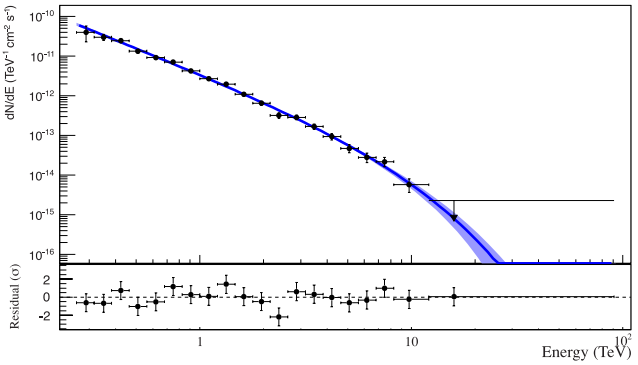

Figure 2. VHE γ-ray spectrum of HESS J1640−465 (top) and flux residuals (bottom) extracted within the 90 per cent containment radius (see the text). Also shown is the best-fitting power law, plus exponential cut-off model and 68 per cent error band. All spectral points have a minimum significance of 2σ. The last point is the differential flux upper limit in this energy band at 95 per cent confidence level.

2.2 Spectrum

The VHE γ-ray spectrum is shown in Fig. 2 and has been extracted using *std* cuts (60 p.e. minimum image intensity, $E_{\rm th} = 260$ GeV), using the reflected region background method (Berge et al. 2007) and forward folding with a maximum likelihood optimization (Piron et al. 2001) from the 90 per cent containment radius of the VHE γ-ray emission of HESS J1640−465 of $0.^{\circ}18$ around the best-fitting position. The fit of a power law with exponential cut-off: $\mathrm{d}N/\mathrm{d}E = \Phi_0 \times (E/1\ \mathrm{TeV})^{-\Gamma} \mathrm{e}^{-E/E_{\rm c}}$ results in a photon index $\Gamma = 2.11 \pm 0.09_{\rm stat} \pm 0.10_{\rm sys}$, a differential flux normalization at 1 TeV of $\Phi_0 = (3.3 \pm 0.1_{\rm stat} \pm 0.6_{\rm sys}) \times 10^{-12}\ \mathrm{TeV}^{-1}\ \mathrm{cm}^{-2}\ \mathrm{s}^{-1}$ and a cut-off energy of $E_{\rm c} = 6.0^{+2.0}_{-1.2}$ TeV. The systematic errors on flux norm and index for this data set are based on the difference seen between the main and cross-check analysis and are a result of uncertainties in e.g. atmospheric conditions, simulations, broken pixels, analysis cuts or the run selection. The fit probability p for an exponential cut-off power-law model is $p \sim 36$ per cent, whereas the fit probability for a pure power-law model is $p \sim 1$ per cent. The luminosity of HESS J1640−465 above 1 TeV at 10 kpc distance is $L_{>1\rm TeV} \simeq 4.6 \times 10^{35} (d/10\,\mathrm{kpc})^2\ \mathrm{erg\ s}^{-1}$, a factor of ∼2.8 higher than that of the Crab nebula.

The photon index as reconstructed with the new HESS data at TeV energies is compatible with the photon index as reconstructed in the GeV domain (Slane et al. 2010; Nolan et al. 2012; Ackermann et al. 2013). A simultaneous exponential cut-off power-law fit to the GeV data points as derived by Slane et al. (2010) and new TeV data between 200 MeV and 90 TeV (shown in Fig. 3) has been performed. The result of this fit is summarized in Table 1 and shows that the flux at 1 TeV, the photon index as well as the cut-off energy are consistent with the fit to the HESS-only data. The fit has a χ^2 of 21 for 24 degrees of freedom (d.o.f.) with a probability of 63 per cent[2] and implies that no break in the γ-ray spectrum between the

[2] The fit has been performed on the binned H.E.S.S spectrum shown in Fig. 2 and on the GeV spectrum from Slane et al. (2010) taking into account statistical errors only.

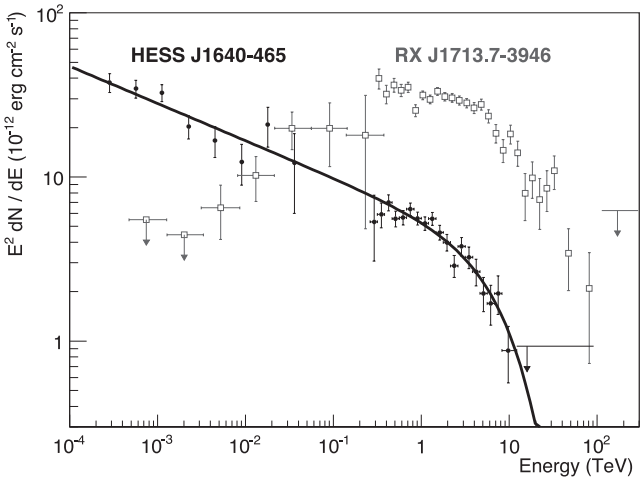

Figure 3. Comparison of the HE and VHE γ-ray spectra of HESS J1640−465 (filled circles) and RX J1713.7−3946 (open squares). Data for RX J1713.7−3946 are from Abdo et al. (2011) and Aharonian et al. (2011), GeV data of HESS J1640−465 are from Slane et al. (2010). Also shown is the best-fitting exponential cut-off power-law model to the full γ-ray spectrum (Table 1).

Fermi and HESS energy range is required in order to describe the data.

3 *XMM–Newton* DATA ANALYSIS

Funk et al. (2007) reported the detection of the candidate PWN XMMU J164045.4−463131 with *XMM–Newton* and introduced it as a potential counterpart of HESS J1640−465. As becomes clear from Fig. 1, the VHE γ-ray emission region also overlaps with the northern part of the shell of SNR G338.3−0.0. To investigate the γ-ray emission scenarios related to the SNR, the *XMM–Newton* data (ObsID: 0302560201) were re-analysed to derive an upper limit for diffuse X-ray emission originating from the northern part of the shell. For the analysis, the Science Analysis System (SAS) version 12.0.1 was used, supported by tools from the FTOOLS package and XSPEC version 12.5.0 (Arnaud 1996) for spectral modelling. The data are affected by long periods of strong background flaring activity resulting in net exposures of only 5.9 ks (PN) and 13.5 ks (MOS), following the suggested standard criteria for good-time-interval filtering. To detect and remove point-like X-ray sources, the standard *XMM–Newton* SAS maximum likelihood source detection algorithm was used in four energy bands [(0.5–1.0), (1.0–2.0), (2.0–4.5) and (4.5–10.0) keV]. Events around all sources detected in any of these bands were removed from a region corresponding to the 95 per cent containment radius of the *XMM–Newton* PSF at the respective source position in the detector. The total flux upper limit was derived assuming that the remaining count rate from a polygon region enclosing the northern part of the shell is due to background. A power-law model with photon index $\Gamma_X = -2$ was applied to constrain non-thermal leptonic emission. Two different absorption column densities as found in the literature, $N_{\rm H,\,1} = 6.1\times10^{22}$ cm^{-2} (Funk et al. 2007) and $N_{\rm H,2} = 1.4\times10^{23}$ cm^{-2} (Lemiere et al. 2009), have been considered. No diffuse X-ray emission coincident with the SNR shell was detected with this data set. The resulting 99 per cent confidence upper limits for the unabsorbed flux [(2–10) keV] are $F_{99}(N_{\rm H,1}) = 4.4 \times 10^{-13}$ erg cm^{-2} s^{-1} and $F_{99}(N_{\rm H,2}) = 8.3 \times 10^{-13}$ erg cm^{-2} s^{-1}. These values have been scaled up by 11 per cent to account for the missing area due to excluded point-like sources.

4 DISCUSSION

The HESS source encloses the PWN candidate XMMU J164045.4−463131 as well as the northwestern (NW) half of the incomplete shell of G338.3−0.0. The comprehensive multiwavelength data available together with the new HESS and *XMM–Newton* results allow for a much more detailed investigation of the SED and hence the underlying non-thermal processes to be carried out. As the evolutionary state of G338.3−0.0 is essential for the discussion, the age of the SNR is estimated, and the environment in which it likely expanded is investigated. These estimates will form the basis for the discussion of the origin of the non-thermal emission in a PWN and SNR scenario.

4.1 Age and environment of G338.3−0.0

The age and environment of the SNR have a large influence on the interpretation and modelling of the emission scenario and thus deserve discussion in this context. Previous estimates put the age of the SNR in the range of (5–8) kyr (Slane et al. 2010); however, as becomes evident from the discussion below, it may be significantly younger than that.

If the X-ray PWN is indeed related to the SNR, then G338.3−0.0 originated from a core-collapse supernova (SN) explosion of a massive star. Such stars usually modify the surrounding medium through strong stellar winds, creating a cavity of relatively low density surrounded by a high-density shell of swept-up material. (see Weaver et al. 1977; Chevalier 1999). Such a wind-blown bubble scenario has never been considered for this object, but needs to be explored for a detailed discussion of the γ-ray emission mechanisms possibly at work in HESS J1640−465. These cavities have significant impact on the evolution of the subsequent SN shock front, and such scenarios have been evoked to explain the properties of other SNRs like the Cygnus Loop (e.g. Levenson et al. 1998), RCW 86 (Vink, Kaastra & Bleeker 1997) and RX J1713.7−3946 (Fukui et al. 2003), all of which have physical diameters similar to G338.3−0.0. Chevalier (1999) estimated the size of wind-blown cavities by requiring a pressure equilibrium between the inside of the bubble, which has been pressurized by the total energy of the wind: $1/2\dot{M}v_{\rm w}^2\tau$, and the surrounding medium. Here, $\dot{M}$ is the mean mass-loss rate, $v_{\rm w}$ is the wind speed and τ is the lifetime of the star. With a distance of 10 kpc, the radius of the observed shell of G338.3−0.0 is 10 pc, which is assumed here to be comparable to the size of the wind-blown bubble. Such sizes can be achieved by a typical $\sim$20 M$_\odot$ O-type star with $\tau \simeq 7$ Myr, $\dot{M} \simeq 10^{-7}$ M$_\odot$ yr^{-1} and $v_{\rm w} \simeq 2600$ km s^{-1}, evolving in an H II region with temperature 10 kK (Osterbrock 1989) and average density of $n \sim 150$ cm^{-3} (see below; Kudritzki & Puls 2000; Muijres et al. 2012). This corresponds to a total mass-loss in the main-sequence phase of 0.7 M$_\odot$. An extreme case that may provide a lower limit to the age of the SNR can be derived by the assumption that the remaining material inside the cavity solely originates from the stellar wind. The mean number density then is $n_0 \sim 0.01$ cm^{-3} with a total mass swept up by the SNR shock of 0.7 M$_\odot$. This means that the SNR shock would evolve freely expanding up to the radius of the wind-blown bubble. Assuming average shock velocities between (5000–10 000) km s^{-1}, the age of the SNR would be (1–2) kyr, which is considerably younger than the estimate of (5–8) kyr by Slane et al. (2010), owing to the lower density.

In addition to the SNR age, also the density of the ISM in the immediate vicinity of the shock region has major impact on the interpretation of the emission scenario. The density in the shell

Table 1. Best-fitting spectrum results of the new HESS data as shown in Fig. 2, and in combination with the GeV spectrum from Slane et al. (2010).

Data	$E_{\rm min}$	$E_{\rm max}$	Γ	Φ_0 (10^{-12} cm^{-2} s^{-1})	$E_{\rm c}$ (TeV)
HESS	260 GeV	90 TeV	2.11 ± 0.09	3.3 ± 0.1	$6.0^{+2.0}_{-1.2}$
HESS + *Fermi*-LAT	200 MeV	90 TeV	2.23 ± 0.01	3.7 ± 0.2	$8.8^{+2.3}_{-1.5}$

surrounding the wind-blown bubble can be estimated with various methods, i.e. via thermal radio emission, thermal X-ray measurements and H I absorption studies. Castelletti et al. (2011) found evidence for thermal radio emission in the SNR shell indicating the presence of dense material. The authors infer electron densities based on the free–free absorption feature in the radio spectrum of $n_{\rm e} \sim (100–165)$ cm^{-3}. No diffuse X-ray emission from the SNR shell have been reported in Funk et al. (2007), and in the previous section, upper limits have been derived. Slane et al. (2010) argue that therefore high gas densities are not supported. However, the lack of observed thermal X-ray emission might be consistent with the very large distance and high column densities inferred from the *XMM–Newton* and *Chandra* spectra (Lemiere et al. 2009) of the PWN XMMU J164045.4−463131, especially if the plasma temperature is below 1 keV. Only for higher temperatures, as e.g. observed from Kes 32 (Vink 2004), could observable thermal X-rays be expected from this source. Particularly, SNRs evolving rapidly inside low-density wind-blown cavities are not expected to produce significant thermal X-ray emission. Only when the SNR shock hits the surrounding shell, the medium in the shock region thermalizes rapidly and cools extremely fast, which makes the SNR an efficient emitter of hard thermal X-rays, but only during a short time. Later, the temperatures are expected to drop significantly below 1 keV due to the decreased shock speeds of only a few 100 km s^{-1} (see e.g. Tenorio-Tagle et al. 1991). As outlined above, due to the high absorption towards G338.3−0.0 such emission is not expected to be detectable.

Finally, the H I absorption feature can be used to infer a maximum (neutral) gas density. Assuming that all of the H I gas as studied by Lemiere et al. (2009) between −65 and −55 km s^{-1} is associated with G338.3−0.0 and located in a shell with 4 pc thickness (as supported by radio observations) at 10 kpc, a maximum density of $n_{\rm H,max} \simeq 600$ cm^{-3} can be derived. However, since some of the absorbing gas may not be associated with G338.3−0.0, average neutral gas densities $\bar{n}_{\rm H}$ lower than that are also plausible. From the H I absorption measurements and the thermal radio emission, the hydrogen gas (neutral plus ionized) in the region is consistent with densities of $\bar{n}_{\rm H} \gtrsim (100–150)$ cm^{-3}. Purcell et al. (2012) performed a survey for high-density gas ($n \gtrsim 10^4$ cm^{-3}) in NH_3 transition lines in the Galactic plane. With the sensitivity of this survey and given that no emission in these transition lines is seen towards HESS J1640−465, a molecular cloud more massive than ∼8000 M$_\odot$ is not supported by the data. However, this does not exclude the existence of smaller, similarly dense clumps of material in the shell region (see below). There is also no maser emission detected towards the TeV emission, which would have indicated the interaction of a shock wave with dense material (e.g. Walsh et al. 2011).

4.2 PWN scenario

The positional coincidence of HESS J1640−465 and 2FGL 1640.5−4633 with the candidate X-ray PWN XMMU J164045.4−463131 is seen as evidence for leptonic γ-ray emission from a PWN (Funk et al. 2007; Lemiere et al. 2009; Slane et al. 2010). In these scenarios, electrons are accelerated to energies of hundreds of TeV in the PWN, radiate via synchrotron and IC processes, and produce the observed X-ray and HE and/or VHE γ-ray emission. In the following, the PWN interpretation will be confronted with the new spectral and morphological HESS results and the available multiwavelength information.

The γ-ray spectrum of middle-aged and old PWNe is characterized by a break in the SED of $\Delta\Gamma = 0.5$ at the energy where the IC/synchrotron loss time of the parent electron population is similar to the age of the source (e.g. Hinton & Hofmann 2009). For young PWNe ($t \simeq 1$ kyr), the γ-ray spectrum from interactions of electrons with magnetic and radiation fields is effectively uncooled up to the cut-off energy as IC and synchrotron loss times are much longer in a typical PWN environment. This leads to a peak in the IC and synchrotron spectra at energies just below the cut-off energy in the electron spectrum. An IC peak (or spectral break) is seen for all of the GeV and TeV identified PWNe (e.g. Aharonian et al. 2005, 2006b; Abdo et al. 2010c; Grondin et al. 2011; Abramowski et al. 2012a), but not for HESS J1640−465. To reproduce the observed γ-ray spectral index $\Gamma_\gamma \simeq 2.2$ for a young object ($\lesssim$2.5 kyr), the injection spectrum has to be $\Gamma_{\rm e} = 3.4$, as $\Gamma_{\rm e} = (2\Gamma_\gamma - 1)$ – an index significantly steeper than predicted by *Fermi* acceleration theory. Slane et al. (2010) suggested an additional Maxwellian low-energy electron component in order to explain the smooth connection of the HE and VHE γ-ray spectra. As shown in Section 2.2, the new high-quality HESS spectrum connects with the GeV spectrum without any discernable features and thus does not require such a contribution. In fact, a χ^2 test of the Slane et al. (2010) model on the binned GeV and TeV spectrum results in a $\chi^2 = 189$ for 25 d.o.f. with very low probability, not supporting a significant contribution of such a Maxwellian component. This can be compared to the exponential cut-off power-law model as shown in Table 1, which has a $\chi^2 = 21$ for 24 d.o.f.

From a theoretical point of view, the extent of the PWN is expected to be smaller than its associated SNR (e.g. Blondin, Chevalier & Frierson 2001). This prediction is supported by observations of several PWNe, including MSH 15−52 (Aharonian et al. 2005) and Vela X (Abramowski et al. 2012a). The intrinsic size of HESS J1640−465 at TeV energies, however, is larger than G338.3−0.0 and features significant overlap with the shell of the SNR – a behaviour that is not seen for any other PWN.

At radio wavelengths, Castelletti et al. (2011) derived upper limits on the possible radio emission from the PWN at various wavelengths, with the most constraining limit of 3.7×10^{-17} erg cm^{-2} s^{-1} at 610 MHz within the X-ray PWN. Due to the different cooling times of the underlying electron population, the PWN is expected to have a larger extent in radio than in X-rays (e.g. Gaensler & Slane 2006). As no radio emission has been detected at the X-ray PWN location, it is hard to estimate the size and hence total flux from a potential radio PWN. The 610 MHz map shows a deficit of emission at the X-ray PWN location and some enhancement inside the rest of the SNR. This could be associated with projected SNR emission,

or with a relic radio PWN. For young PWNe, the peak of the radio emission is expected to be close to the pulsar position. Since the radio surface brightness around the putative pulsar is much lower compared to the rest of the SNR interior, this would imply that the radio excess is related to projected shell emission. For older systems, however, the radio PWN can very well fill the full interior of the SNR shell. As a compromise, the limit as given by Castelletti et al. (2011) is scaled up by a factor of 16 to cover the interior of the SNR shell. In this case, the radio limit is a factor of ∼5 below the model curves in Lemiere et al. (2009) and Slane et al. (2010), and would imply a low-energy cut-off of the underlying electron spectrum significantly higher than the 50 GeV as used by Lemiere et al. (2009).

In summary, the interpretation of the GeV and TeV emission as solely originating from a PWN is very difficult as neither the γ-ray spectrum nor the morphology or the radio data support such a picture. A possible solution would be that the GeV emission has a different origin than the TeV emission. This, however, requires fine-tuning to explain the smooth *Fermi* and HESS spectrum, and the positional coincidence of the GeV and TeV sources. Also, the TeV spectrum alone does not show any significant deviation from a pure power law below the cut-off energy, which would be expected for a young PWN. In fact, the radio upper limit in Castelletti et al. (2011), the X-ray data and a non-dominant IC component in the γ-ray regime would be consistent with XMMU J164045.4−463131 being a young PWN (cf. fig. 5 of Funk et al. 2007). In general, the featureless γ-ray spectrum over almost six decades in energy is challenging for any leptonic model as spectral breaks and sharp cut-offs are expected in the resulting SED due to cooling and Klein–Nishina effects, respectively (e.g. Hinton & Hofmann 2009).

The TeV emission also significantly overlaps with the NW part of the shell of G338.3−0.0 and it is hence quite natural to explore an origin of the non-thermal emission in the SNR shell. Especially, the spectral characteristics of HESS J1640−465 are similar to that of prominent Galactic SNRs interacting with molecular clouds such as W28, W51C or IC 443 (see Ohm 2012, and references therein). In the following, the focus will be on an origin of the non-thermal emission in the SNR shell, bearing in mind that some fraction of the total TeV emission could plausibly originate from the PWN.

4.3 SNR scenario

Given the spectral and morphological similarity of HESS J1640−465 with other Galactic SNRs interacting with molecular clouds, an SNR origin of the non-thermal emission is studied in the following. In a hadronic γ-ray emission scenario, a high density is required to provide sufficient target material for the relativistic protons to produce neutral pions which subsequently decay into energetic photons (see e.g. Aharonian, Drury & Voelk 1994). This high-density material outside the SNR shock could either be the wind shell surrounding the stellar-wind bubble or the dense material known to exist in the vicinity of HESS J1640−465. The relatively low ISM density inside the wind-blown bubble would not be sufficient to account for the bulk of the observed γ-ray emission, and thus the target material must be of different origin. In the environment of G338.3−0.0, there could be at least two possibilities for the occurrence of sufficiently dense ISM: (a) As discussed in Section 4.1 and following Chevalier (1999), wind-blown bubbles are surrounded by a thin dense shell containing the bulk of the material swept up by the stellar wind. If the expanding shock of G338.3−0.0 is now close to this region, accelerated protons might interact with this dense material and subsequently produce the observed γ-rays. (b) A second possibility is that the SNR shock expands into a highly inhomogeneous ISM towards the nearby H II region featuring dense clumps of molecular gas surrounded by regions of comparatively low density. Here, the particles could be efficiently accelerated within the inter-clump medium while energetic protons can penetrate into the dense clumps and produce the observed γ-ray emission. This scenario has already been proposed for the young (∼2 kyr) VHE γ-ray emitting SNR RX J1713.7−3946 (see Zirakashvili & Aharonian 2010) where dense molecular cloud cores have been detected in the shock region (e.g. Sano et al. 2010). Such ISM conditions are probably also present in the vicinity of G338.3−0.0, due to its vicinity to a massive and dense H II region, making this emission scenario also viable for HESS J1640−465.

In contrast to middle-aged interacting SNRs like IC 443 (Abdo et al. 2010b) and W 44 (Abdo et al. 2010a) where the γ-ray spectra are strongly peaked at GeV energies, RX J1713.7−3946 and other young SNRs emit a large fraction of their HE emission in the TeV regime, either due to a different radiation process or their earlier stage in evolution. Fig. 3 shows a comparison between the GeV–TeV spectra of HESS J1640−465 and RX J1713.7−3946 as seen by *Fermi* and HESS Interestingly, their spectral shapes in the TeV regime are very similar, which could support an age younger than (10–20) kyr for G338.3−0.0. However, the GeV spectrum becomes much harder for RX J1713.7−3946 but keeps the same slope for HESS J1640−465. Leptonic models giving rise to the observed shape of the γ-ray spectrum of RX J1713.7−3946 have been discussed in the literature quite extensively (see e.g. Abdo et al. 2011; Yuan et al. 2011). However, following Zirakashvili & Aharonian (2010), the change in slope towards lower energies for RX J1713.7−3946 could also be explained in a hadronic scenario by the smaller penetration depths in the dense molecular cloud cores for protons with lower energies (see also Inoue et al. 2012). These particles therefore cannot interact with the same amount of material as protons with higher energies, giving rise to an underluminous and harder GeV γ-ray spectrum. The fact that this feature is not seen for HESS J1640−465 might indicate an older remnant than e.g. RX J1713.7−3946 (i.e. $\gtrsim$2.5 kyr) or different diffusion properties of the local ISM that allow also low-energy protons to fully penetrate the dense molecular clumps. An age of 2.5 kyr would imply some mixing of the stellar-wind material and the ISM leading to average densities in the wind bubble of $n_0 \sim 0.1$ cm^{-3} (cf. Section 4.1).

When comparing the TeV morphology of HESS J1640−465 to G338.3−0.0 (Fig. 1), it becomes clear that γ-ray emission only shows significant overlap with the NW part of the radio shell. Thus, in a hadronic scenario, the lack of emission from the south-eastern (SE) shell needs to be explained. In such a model, the γ-ray emission is expected to follow the distribution and the density of available target material in the shock region. Indeed, a correlation between the molecular and atomic gas and the VHE γ-ray intensity from RX J1713.7−3946 has recently been reported by Fukui et al. (2012). Thus, if dense target material is much more abundant in the northern region of G338.3−0.0 compared to the south, the observed TeV morphology of HESS J1640−465 is consistent with a hadronic scenario. Fig. 4 shows the *Spitzer* MIPS (Rieke et al. 2004) 24 μm image of this region, which essentially traces the abundance of interstellar dust and dense H II star-forming regions. Here, it can be seen that the mean infrared intensity towards the NW part is a factor of ∼5 higher than towards the SE area of the shell. Therefore, the different densities could indeed give rise to the observed morphology. To further test the hypothesis of the NW shell being the origin of the VHE γ-ray emission, only this part of the radio shell was used as a template and convolved with the HESS PSF. The resulting

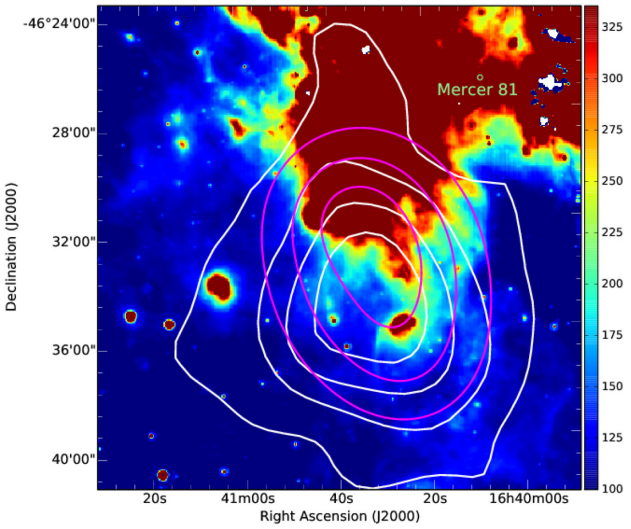

Figure 4. *Spitzer* MIPS 24 μm image in units of MJy sr^{-1} with overlaid contours from the smoothed HESS excess map (white) and contours of the NW part of the SNR shell from the 610 MHz image, convolved with the HESS PSF (magenta, cf. Fig. 1).

contours are overplotted on the *Spitzer* image in Fig. 4 and show a good agreement with the VHE γ-ray excess contours from HESS

Fig. 5 shows the measured SED of G338.3−0.0 along with the new HESS data and *XMM–Newton* limits. Also shown is a single-zone time-dependent model for the continuous injection of electrons and protons over an assumed age of G338.3−0.0 of 2.5 kyr (e.g. Funk et al. 2007). HE electrons produce synchrotron and IC γ-ray emission in interactions with magnetic and radiation fields, respectively. HE protons produce π^0-decay γ-ray emission in interactions with material in the SNR shell. The broad-band SED can be explained in this scenario with a reasonable choice of input parameters. The leptonic component can be constrained by the observed synchrotron spectrum from radio to X-rays. In this model calculation, a magnetic field of $B = 35\,\mu$G, maximum electron energy of $E_{c,e} = 10$ TeV and electron spectral index of $\Gamma_e = 2.0$ are required to reproduce the radio spectrum and to not violate the X-ray limit. The target radiation fields have been chosen based on Lemiere et al. (2009), with a dust component that has been increased to account for the five times higher radiation field energy density in the northern part of the shell. It is clear from Fig. 5 that the predicted IC emission is at least two orders of magnitude below the observed γ-ray emission for an assumed electron-to-proton (e/p) ratio of 10^{-2}. Furthermore, the smooth connection of the HE and VHE γ-ray spectrum cannot be explained. A considerably higher e/p ratio of $\simeq$0.1 (and lower magnetic field of $B \simeq 10\,\mu$G) is required to reach the TeV flux. Even in this case, the IC spectral shape and maximum energy are not supported by the VHE γ-ray spectrum. In dense environments, bremsstrahlung can significantly contribute to the non-thermal emission. Densities as high as 500 cm^{-3} and e/p ratios of 0.1 are, however, required to reach the flux observed by HESS

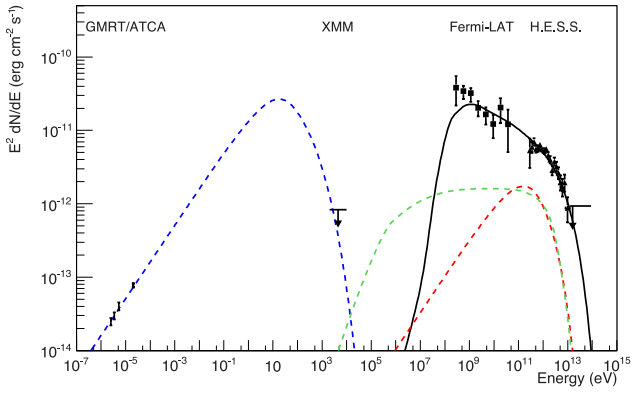

Figure 5. HE and VHE γ-ray spectrum of HESS J1640−465 as given in Slane et al. (2010) and shown in Fig. 2, respectively. The X-ray limit has been derived in the northern part of the radio shell and assuming the higher column density as derived by Lemiere et al. (2009) (see Fig. 1 and the text), and the radio data are from Castelletti et al. (2011), scaled by a factor of 0.5, assuming that half of the radio emission comes from the northern part of the shell. The long dashed blue and red dash–dotted curves represent synchrotron and IC emission from non-thermal electrons, respectively. The green dashed curve represents the bremsstrahlung component and the solid black curve represents the hadronic π^0-decay γ-ray emission.

In a hadronic scenario, a total energy transferred into protons of $W_p = 2.5 \times 10^{50}$ erg, maximum proton energy $E_{c,p} = 50$ TeV and spectral index of $\Gamma_p = 2.2$ as well as an average ambient density $\bar{n}_H = 150$ cm^{-3} are required to reproduce the GeV–TeV spectrum. The measured TeV flux coupled with the large estimated distance of ∼10 kpc would imply that HESS J1640−465 is the most luminous Galactic VHE γ-ray SNR detected so far [$L_{>1\,\mathrm{TeV}} \simeq 4.6 \times 10^{35}(d/10\,\mathrm{kpc})^2$ erg s^{-1}] . The TeV luminosity is therefore about one order of magnitude higher than that of the W51C SNR (Aleksić et al. 2012). Due to the harder γ-ray spectral index, HESS J1640−465 has a total γ-ray luminosity comparable to W51C. The product of total energy in interacting protons and mean ambient density of $W_p\bar{n}_H \simeq 4 \times 10^{52}(d/10\,\mathrm{kpc})^2$ erg cm^{-3} requires a considerable amount of SN kinetic energy that is transferred to HE protons and/or a high average density of the target material as motivated before. With the gas densities estimated above, a very large energy in protons is needed to reach the measured GeV and TeV flux. This implies that either the SN explosion was as energetic as $E_{SN} \simeq 4 \times 10^{51}(d/10\,\mathrm{kpc})^2$ erg (assuming that a canonical 10 per cent of SN explosion energy is channelled into cosmic rays) and/or that the fraction of E_{SN} transferred into relativistic protons is significantly larger than the canonical 10 per cent, i.e. up to $\sim 40\,(d/10\,\mathrm{kpc})^2$ per cent for a typical $E_{SN} = 10^{51}$ erg. Note that this estimate can be even higher, as only the northern half of the SNR shell seems to be illuminated by cosmic rays.

5 CONCLUSIONS AND OUTLOOK

The detailed HESS results presented in this work show that the VHE γ-ray emission from HESS J1640−465 significantly overlaps with the NW part of the SNR shell of G338.3−0.0. Moreover, the VHE γ-ray spectrum smoothly connects with the *Fermi* spectrum and has a HE cut-off that implies that particles with tens of TeV energies are present in the acceleration region. The TeV morphology, new radio measurements and the overall γ-ray spectrum are hard to explain in a scenario where most of the non-thermal emission is coming from the PWN. The broad-band SED and morphology of the non-thermal emission from HESS J1640−465 can be better explained in a scenario where protons are accelerated in the shell of G338.3−0.0 and interact with dense gas associated with the G338.4+0.1 H II complex. In this case, the product of total energy in interacting protons and mean ambient density $W_p\bar{n}_H \sim 4 \times 10^{52}(d/10\,\mathrm{kpc})^2$ erg cm^{-3} required to explain the flux measured by *Fermi* and HESS is comparable to the γ-ray-emitting SNR W51C, although the TeV

luminosity of HESS J1640−465 is an order of magnitude higher. In this picture, the non-detection of thermal X-rays is consistent with the large distance to G338.3−0.0 and the high column density along the line of sight. High-resolution and high-sensitivity molecular line observations in this region are required to locate the dense gas that might act as target material and to put limits on the explosion energy of G338.3−0.0. The future Cherenkov Telescope Array with its much better angular resolution and sensitivity is needed to further resolve the VHE γ-ray emission region(s) of HESS J1640−465 and to distinguish the contribution from the SNR shell and the PWN in G338.3−0.0.

ACKNOWLEDGEMENTS

The support of the Namibian authorities and of the University of Namibia in facilitating the construction and operation of HESS is gratefully acknowledged, as is the support by the German Ministry for Education and Research (BMBF), the Max Planck Society, the French Ministry for Research, the CNRS-IN2P3 and the Astroparticle Interdisciplinary Programme of the CNRS, the UK Science and Technology Facilities Council (STFC), the IPNP of the Charles University, the Czech Science Foundation, the Polish Ministry of Science and Higher Education, the South African Department of Science and Technology and National Research Foundation and by the University of Namibia. We appreciate the excellent work of the technical support staff in Berlin, Durham, Hamburg, Heidelberg, Palaiseau, Paris, Saclay and in Namibia in the construction and operation of the equipment. SO acknowledges the support of the Humboldt foundation by a Feodor-Lynen research fellowship. We are also grateful to Gabriela Castelletti, who kindly provided the 610 MHz map and Patrick Slane for the PWN model curve. The authors would also like to thank the anonymous referee for her/his detailed and constructive comments, which significantly improved the quality of this paper. This work is based in part on observations made with the *Spitzer* Space Telescope, which is operated by the Jet Propulsion Laboratory, California Institute of Technology under a contract with NASA.

REFERENCES

Abdo A. A. et al. (Fermi-LAT Collaboration), 2010a, Science, 327, 1103
Abdo A. A. et al. (Fermi-LAT Collaboration), 2010b, ApJ, 712, 459
Abdo A. A. et al. (Fermi-LAT Collaboration), 2010c, ApJ, 714, 927
Abdo A. A. et al. (Fermi-LAT Collaboration), 2011, ApJ, 734, 28
Abramowski A. et al. (HESS Collaboration), 2012a, A&A, 548, A38
Abramowski A. et al. (HESS Collaboration), 2012b, A&A, 548, A46
Ackermann M. et al., (Fermi-LAT Collaboration), 2013, ApJS, 209, 34
Aharonian F. A., Drury L. O., Voelk H. J., 1994, A&A, 285, 645
Aharonian F. et al. (HESS Collaboration), 2005, A&A, 435, L17
Aharonian F. et al. (HESS Collaboration), 2006a, A&A, 457, 899
Aharonian F. et al. (HESS Collaboration), 2006b, A&A, 460, 365
Aharonian F. et al. (HESS Collaboration), 2006c, ApJ, 636, 777
Aharonian F. et al. (HESS Collaboration), 2011, A&A, 531, C1
Aleksić J. et al. (MAGIC Collaboration), 2012, A&A, 541, A13
Arnaud K. A., 1996, in Jacoby G. H., Barnes J., eds, ASP Conf. Ser. Vol. 101, Astronomical Data Analysis Software and Systems V. Astron. Soc. Pac., San Francisco, p. 17
Berge D., Funk S., Hinton J., 2007, A&A, 466, 1219
Blondin J. M., Chevalier R. A., Frierson D. M., 2001, ApJ, 563, 806
Carrigan S. et al. (HESS Collaboration), 2013, preprint (arXiv:1307.4690)
Castelletti G., Giacani E., Dubner G., Joshi B. C., Rao A. P., Terrier R., 2011, A&A, 536, A98
Chevalier R. A., 1999, ApJ, 511, 798
Davies B., de La Fuente D., Najarro F., Hinton J. A., Trombley C., Figer D. F., Puga E., 2012, MNRAS, 419, 1860
de Naurois M., Rolland L., 2009, Astropar. Phys., 32, 231
Freeman P., Doe S., Siemiginowska A., 2001, in Starck J.-L., Murtagh F. D., eds, Proc. SPIE Conf. Ser., Vol. 4477, Astronomical Data Analysis. SPIE, Bellingham, p. 76
Fukui Y. et al., 2003, PASJ, 55, L61
Fukui Y. et al., 2012, ApJ, 746, 82
Funk S., Hinton J. A., Pühlhofer G., Aharonian F. A., Hofmann W., Reimer O., Wagner S., 2007, ApJ, 662, 517
Gaensler B. M., Slane P. O., 2006, ARA&A, 44, 17
Grondin M.-H. et al., 2011, ApJ, 738, 42
Hinton J. A., Hofmann W., 2009, ARA&A, 47, 523
Inoue T., Yamazaki R., Inutsuka S.-i., Fukui Y., 2012, ApJ, 744, 71
Kudritzki R.-P., Puls J., 2000, ARA&A, 38, 613
Lemiere A., Slane P., Gaensler B. M., Murray S., 2009, ApJ, 706, 1269
Levenson N. A., Graham J. R., Keller L. D., Richter M. J., 1998, ApJS, 118, 541
Muijres L. E., Vink J. S., de Koter A., Müller P. E., Langer N., 2012, A&A, 537, A37
Nolan P. L. et al. (Fermi-LAT Collaboration), 2012, ApJS, 199, 31
Ohm S., 2012, in Aharonian F. A., Hofmann W., Rieger F. M., eds, AIP Conf. Ser. Vol. 1505, High Energy Gamma-Ray Astronomy. Am. Inst. Phys., New York, p. 64
Ohm S., van Eldik C., Egberts K., 2009, Astropart. Phys., 31, 383
Osterbrock D. E., 1989, Astrophysics of Gaseous Nebulae and Active Galactic Nuclei. University Science Books, Mill Valley, CA
Oya I. et al. (HESS Collaboration), 2013, preprint (arXiv:1303.0979)
Piron F. et al., 2001, A&A, 374, 895
Purcell C. R. et al., 2012, MNRAS, 426, 1972
Rieke G. H. et al., 2004, ApJS, 154, 25
Sano H. et al., 2010, ApJ, 724, 59
Slane P., Castro D., Funk S., Uchiyama Y., Lemiere A., Gelfand J. D., Lemoine-Goumard M., 2010, ApJ, 720, 266
Spitkovsky A., 2008, ApJ, 682, L5
Tenorio-Tagle G., Rozyczka M., Franco J., Bodenheimer P., 1991, MNRAS, 251, 318
Vink J., 2004, ApJ, 604, 693
Vink J., Kaastra J. S., Bleeker J. A. M., 1997, A&A, 328, 628
Walsh A. J. et al., 2011, MNRAS, 416, 1764
Weaver R., McCray R., Castor J., Shapiro P., Moore R., 1977, ApJ, 218, 377
Whiteoak J. B. Z., Green A. J., 1996, A&AS, 118, 329
Yuan Q., Liu S., Fan Z., Bi X., Fryer C. L., 2011, ApJ, 735, 120
Zirakashvili V. N., Aharonian F. A., 2010, ApJ, 708, 965

This paper has been typeset from a TEX/LATEX file prepared by the author.